International Journal of Natural and Engineering Sciences 8 (1): 32-41, 2014
ISSN: 1307-1149, E-ISSN: 2146-0086, www.nobel.gen.tr

A Comparative Study for Rotor Side Converter Controller of a DFIG-Based Wind Turbine, Using Direct Power Control, Carrier-Based PWM Voltage Control and Hysteresis Current Control Strategies

Mohsen GHORBANI[1*] Babak MOZAFFARI[1] Soodabeh SOLEYMANI[1]
[1] Department of Electrical Engineering, Science and Research Branch, Islamic Azad University, Tehran, Iran

*Corresponding author:
E-mail: ghorbani_m7@yahoo.com

Received: March 16, 2014
Accepted: April 27, 2014

Abstract

This paper investigates and studies the voltage source converter controller performance of a doubly-fed induction generator (DFIG) by using three control methods based on direct power control (DPC), carrier based pulse width modulation (CB-PWM) voltage control and hysteresis current control, and then the results have been compared with each other in different scenarios. This paper focuses on the rotor side converter control of the DFIG, aiming at active and reactive power outputs control, to demonstrate the effectiveness of the control strategies. First simulation section shows the performance of mentioned strategies during variation of rotor speed, from sub-synchronous to super-synchronous. In the second section the value of stator resistance, applied in simulation, have been allocated 70% and 130% of the rated value to determine the robustness of methods despite the error in stator resistance value estimation. In the next scenario, the DFIG is assumed in torque control mode which the input mechanical power of DFIG is provided by a wind turbine. Finally the benefits and drawbacks of methods have been evaluated. The simulation has been accomplished by PSCAD/EMTDC software and the generator rated power is 2^{MW}.

Keywords: Wind turbine, Doubly-fed induction generator, Direct power control, Carrier based pulse width modulation, Hysteresis current control, Voltage source converter (VSC).

INTRODUCTION

Power electronic systems are frequently used for electrical power conversion at a wind turbine generator level, wind farm level or both. The variable speed wind turbines are divided to wind turbines with doubly-fed induction generators (DFIG) and the ones with fully rated converter which is based on synchronous or induction generator.

In the DFIG based wind generator, the power electronic equipment only has to handle a fraction (20–30%) of the total system power which has less power losses and consequently lower converter cost comparing with fully rated converter. Also comparing with fixed speed generators, DFIG can be operated in generation mode at the range of 20% to 30% synchronous speed that enables the power control. [1-3].

The variable-frequency rotor supply from the converter enables the rotor mechanical speed to be decoupled from the synchronous frequency of the electrical network, thereby allowing variable-speed operation of the wind turbine. [4]
This generator has brushes and slip rings for creating the current path to the rotor and variable-speed operation is obtained by injecting a controllable voltage into the rotor at the desired slip frequency. When the generator works in super-synchronous speed, power will be delivered from the rotor, through the converters, to the network and when the generator operates in sub-synchronous mode, the rotor will absorb power from the network. These two operation modes are illustrated in Figure 1, where ω_s is the synchronous speed of the stator field and ω_r is the rotor speed. [5]

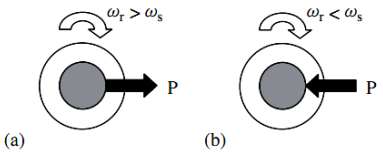

Figure 1. (a) Super-synchronous and (b) sub-synchronous operation of the DFIG wind turbine[5]

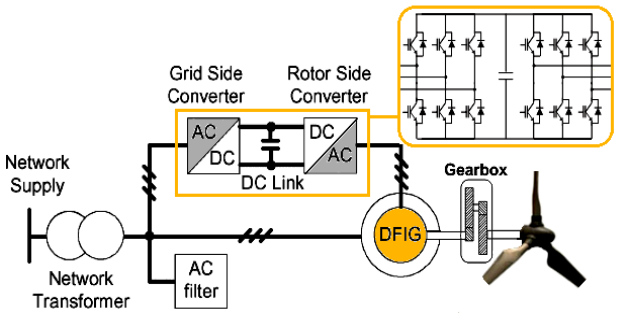

Figure 2. Schematic diagram of the DFIG-based wind energy generation system

The structure of DFIG based wind turbine scheme has been shown in Figure 2. The power converter is made up of a back-to-back converter consists of two converters, i.e., rotor-side converter and grid-side converter. Between the two converters a dc-link capacitor is placed, as energy storage, in order to keep the voltage variations in the dc-link voltage.

With the rotor-side converter it is possible to control the torque or the active power or the speed of the DFIG and also the reactive power or stator terminals voltage, and the main purpose of the grid-side converter is to keep the dc-link voltage in a constant level. [5, 6]

During recent decades, different strategies for controlling the active and reactive power flow between the doubly-fed induction generator and the network have been offered, the most important control methods applied on rotor side converter are direct power control (DPC) presented in [7-10], voltage control using carrier based pulse width modulation (CB-PWM) presented in [11-15] and hysteresis current control cited in [16--19]. Choosing proper control method that increases the statical and dynamical performance is very important.

This paper investigates the mentioned strategies ability in different scenarios including performance of the DFIG during variation of rotor speed from sub-synchronous to super-synchronous, change in applied stator resistance value in simulation, as 70% and 130% rated value and finally analyzing the performance of the DFIG in torque mode. The main consideration in this article is the rotor side converter and control strategy of network side converter has been done by using presented strategy in [11], for fixing the DC link voltage.

METHODS DISCUSSION

In this section we will describe implementation of the previously mentioned methods which are applied on the rotor side converter.

Control of Active and Reactive Power by DPC

Equivalent circuit of DFIG in rotor reference frame which rotates with ω_r is shown in Figure 3 and also relationship between stator and rotor flux in stationary and rotor reference frames is shown in Figure 4.

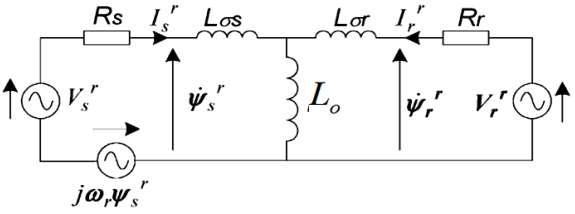

Figure 3. DFIG equivalent circuit in the rotor reference frame [7]

According to Figure 3, stator and rotor flux linkage vectors can be expressed as below:

$$\begin{aligned}\psi_s^r &= L_s I_s^r + L_o I_r^r \\ \psi_r^r &= L_r I_r^r + L_o I_s^r\end{aligned} \quad (1)$$

According to (1), stator current is calculated as (2):

$$I_s^r = \frac{L_r\psi_s^r - L_o\psi_r^r}{L_s L_r - L_o^2} = \frac{\psi_s^r}{\sigma L_s} - \frac{L_o\psi_r^r}{\sigma L_s L_r} \quad (2)$$

Where $\sigma = \left(L_o^2 / L_s L_r\right)$ is leakage coefficient.

From Figure 3 stator voltage vector is determined as:

$$v_s^r = R_s I_s^r + \dot{\psi}_s^r + j\omega_r\psi_s^r \quad (3)$$

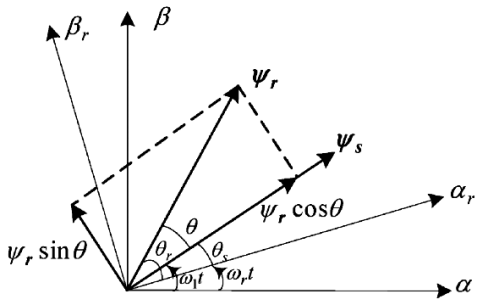

Figure 4. Stator and rotor flux linkage vectors in stationary and rotor reference frames [12]

The stator active power input from the network, neglecting the stator copper loss, is expressed as below: [9]

$$P_s = \frac{3}{2}v_s^r.I_s^r = \frac{3}{2}\left(\dot{\psi}_s^r + j\omega_r\psi_s^r\right)I_s^r \quad (4)$$

Similarly stator reactive power output to the network is expressed as below:

$$Q_s = -\frac{3}{2}v_s^r \times I_s^r = -\frac{3}{2}\left(\dot{\psi}_s^r + j\omega_r\psi_s^r\right)\times I_s^r \quad (5)$$

In considering Figure 4 stator and rotor flux in rotor reference frame can be expressed as:

$$\psi_r^r = |\psi_r^r|.e^{j\theta_r} \quad (6a)$$

$$\psi_s^r = |\psi_s^r|.e^{j\theta_s} \quad (6b)$$

$$\psi_s^r = \psi_s^s.e^{-j\omega_r t} \quad (6c)$$

$$\dot{\theta}_s = \omega_1 - \omega_r \quad (6d)$$

Stator flux in stationary reference frame is determined as below:

$$\psi_s^s = \int \left(v_s^s - R_s I_s^s\right)dt \quad (7)$$

Neglecting the stator winding resistance and by assumption that connected network to stator is stable and rotor speed during sampling does not change (due to high inertia of wind turbine) we will have: [7]

$$|\psi_s^r| = |\psi_s^s e^{-j\omega_r t}| = \left|\int v_s^s dt\right| = constant \Rightarrow \frac{d|\psi_s^r|}{dt} = o \quad (8)$$

By differentiation of the (6a) and by using the (6b) we will have:

$$\dot{\psi}_s^r = |\psi_s^r|\, j\dot{\theta}_s e^{j\theta_s} = j\left(\omega_1 - \omega_r\right)\psi_s^r \quad (9)$$

By substituting of (2) and (9) in (4) and (5), for active and reactive powers of stator: [7]

$$\begin{aligned}P_s &= -\frac{3}{2}\frac{L_o}{\sigma L_s L_r}\omega_1 |\psi_s^r||\psi_r^r|\sin\theta \\ Q_s &= \frac{3}{2}\frac{\omega_1}{\sigma L_s}|\psi_s^r|\left(\frac{L_o}{L_r}|\psi_r^r|\cos\theta - |\psi_s^r|\right)\end{aligned} \quad (10)$$

By derivation of (10) we will have:[7]

$$\frac{dP_s}{dt} = -\frac{3}{2}\frac{L_o}{\sigma L_s L_r}\omega_1 |\psi_s^r| \frac{d\left(|\psi_r^r|\sin\theta\right)}{dt}$$

$$\frac{dQ_s}{dt} = \frac{3}{2}\frac{L_o}{\sigma L_s L_r}\omega_1 |\psi_s^r| \frac{d\left(|\psi_r^r|\cos\theta\right)}{dt} \quad (11)$$

Regarding to (11) it seems that fast changes of active and reactive powers are obtained by changing the $|\psi_r^r|\sin\theta$ and $|\psi_r^r|\cos\theta$ respectively. From Figure 4 it is clear that $|\psi_r^r|\sin\theta$ and $|\psi_r^r|\cos\theta$ is components of rotor flux vector which are respectively perpendicular and conformed with stator flux vector. It shows that if rotor flux changes in direction of stator flux (change of $|\psi_r^r|\cos\theta$), reactive power Q_s changes and if rotor flux changes in vertical direction of stature flux (change of $|\psi_r^r|\sin\theta$), active power P_s changes, primary position of rotor flux and its amplitude has no effect on changes of active and reactive power.

In this method eight special vectors $V_0(000) - V_7(111)$ for rotor side converter is allocated the same as Figure 5.

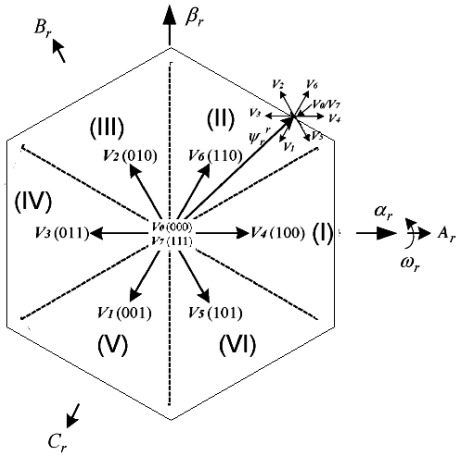

Figure 5. Voltage vectors and the control of flux using voltage vectors[7]

In considering Figure 4, the rotor flux of DFIG in reference frame of rotor is expressed as:

$$\frac{d\psi_r^r}{dt} = V_r^r - R_r I_r^r \quad (12)$$

Equation (12) shows that by neglecting the rotor resistance, the rotor flux changes is determined by applied voltage to rotor, so the rotor flux moves in direction of rotor voltage and its speed changes is proportionated with domain of applied voltage vector. Thus, by choosing a proper voltage vector, movement of rotor flux can be controlled. Choosing the appropriate voltage vector is depended on position of flux linkage.

In this Process, the plate of $\alpha_r - \beta_r$, that rotates in the speed of the rotor, is divided in six area which is shown in Figure 5. The position of eight voltage vectors is also constant to this rotating plate. Also two three-level hysteresis Comparator has been used for producing the active power state (S_p) and reactive power state (S_q) the same as Figure 6.

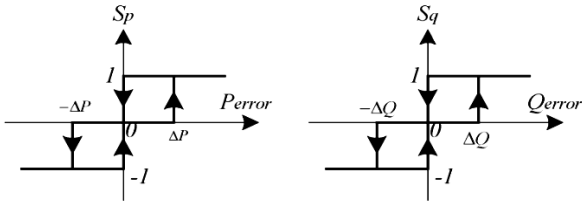

Figure 6. Active and reactive power hysteresis control [7]

The scheme of direct power control method has been shown in the figure 7.

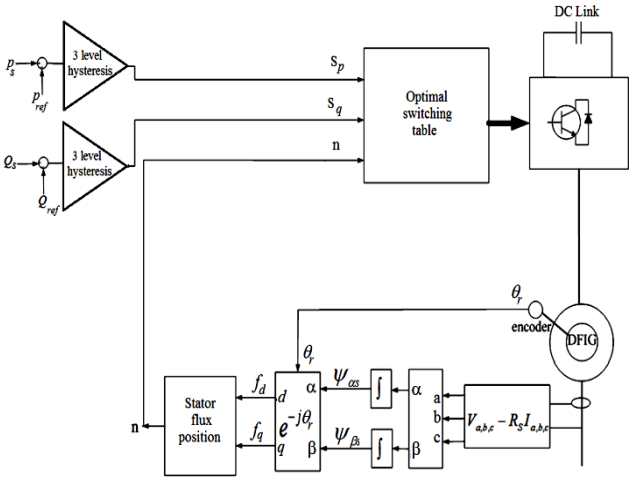

Figure 7. Schematic of the FOC implementation for rotor side converter

According to (11) and by using the output information of hysteresis and stator flux vector position in rotor reference frame, a switching table is presented in Table 1 which includes optimized rotor voltage vectors to decrease the error of active and reactive powers from their reference values.

In this method, due to use of hysteresis controllers and absence of fixed frequency switching pattern, the switching frequency is variable, which creates some problems in designing the filter, moreover the existence of spread harmonic spectrum and ripples in current, will have a bad impact on the system. But due to lack of using any switching pattern, applying this control method is simple. [7-10] Based on these modulation methods, reaction speed in DPC is high.

Table 1. Optimal Switching Table [7]

		I	II	III	IV	V	VI
S_q=1	S_q= 1	101	100	110	010	011	001
	S_q= 0	100	110	010	011	001	101
	S_q=-1	110	010	011	001	101	100
S_q=0	S_q= 1	001	101	100	110	010	011
	S_q= 0	111/000	111/000	111/000	111/000	111/000	111/000
	S_q=-1	010	011	001	101	100	110
S_q= -1	S_q= 1	001	101	100	110	010	011
	S_q= 0	011	001	101	100	110	010
	S_q=-1	010	011	001	101	100	110

Control of Active and Reactive Power by Using Carrier Based Pulse Width Modulation Voltage Control

Field oriented control technique is used as a commonly known method for controlling the DFIG in different references. In this method DFIG has been surveyed in the synchronous reference frame, in which *d* axis of reference frame is aligned with stator flux vector that rotates by synchronous speed and *q* axis is conformed to stator voltage vector.

This technique due to internal current control loops shows good statical and dynamical performance. Current of rotor has been separated to two perpendicular axis, *d* and *q*, in reference frame. The *q* current component is used for active power control or while the *d* current component is used for reactive power control. Active and reactive power of stator is controllable by adjusting the current and voltage of rotor. Therefore, stator active and reactive power control is implemented on rotor side converter. In this strategy, by using the vector control, DFIG power control is performed [11-14]. Under stator-flux orientation, the relationship between the d-q axis voltages, currents and fluxes may be written as:[11]

$$\begin{cases} \psi_s = \psi_{ds} = L_o i_{ms} = L_s i_{ds} + L_o i_{dr} \\ \psi_{qs} = 0 = L_s i_{qs} + L_o i_{qr} \Rightarrow i_{qs} = -\dfrac{L_o}{L_s} i_{qr} \end{cases} \quad (13)$$

$$\begin{cases} \psi_{dr} = \dfrac{L_o^2}{L_s} i_{ms} + \sigma L_r i_{dr} \\ \psi_{qr} = \sigma L_r i_{qr} \end{cases} \quad (14)$$

$$\begin{cases} v_{dr} = R_r i_{dr} + \sigma L_r \dfrac{di_{dr}}{dt} - \omega_{slip} \sigma L_r i_{qr} \\ v_{qr} = R_r i_{qr} + \sigma L_r \dfrac{di_{qr}}{dt} + \omega_{slip} \left(L_m i_{ms} + \sigma L_r i_{dr} \right) \end{cases} \quad (15)$$

Where $\sigma = \left(L_o^2 / L_s L_r\right)$ and $L_m = \left(L_o^2 / L_s\right)$ and $\omega_{slip} = \omega_s - \omega_r$

The active and reactive powers at the terminal of the stator winding can be derived as: [12]

$$\begin{aligned} P_s &= -3\frac{P}{2} \omega_s L_m i_{ms} i_{qr} \\ Q_s &= 3\frac{P}{2} \omega_s L_m i_{ms} i_{ds} \end{aligned} \quad (16)$$

Essentially the measurement of stator and rotor current, stator voltage and position of rotor are required for this process. Whereas, the stator is connected to the network, magnetizing current i_{ms} can be supposed constant.
Angle of stator flux is estimated using the following equation: [11]

$$\begin{aligned} \psi_{\alpha s} &= \int \left(v_{\alpha s} - R_s i_{\alpha s} \right) dt \\ \psi_{\beta s} &= \int \left(v_{\beta s} - R_s i_{\beta s} \right) dt \\ \theta_s &= \tan^{-1} \frac{\psi_{\beta s}}{\psi_{\alpha s}} \end{aligned} \quad (17)$$

Where θ_s is the position of stator flux vector.

According to (16), active power is proper with i_{qr} and can be adjusted by v_{qr} . Also, reactive power has direct relation with i_{ds} and as (13) indicates, i_{ds} is controllable by i_{dr}, with ψ_{ds} unchanged. Therefore, the d-axis component of the rotor current, i_{dr}, and consequently v_{dr} can be controlled to regulate the stator reactive power.

Both references of *q* and *d* rotor current component are obtained with crossing the difference between the measured value and reference value of the active and reactive power (respectively) from the PI controller.

From of rotor voltage in (15), we have:

$$\begin{aligned} v'_{dr} &= R_r i_{dr} + \sigma L_r \frac{di_{dr}}{dt} \\ v'_{qr} &= R_r i_{qr} + \sigma L_r \frac{di_{qr}}{dt} \end{aligned} \quad (18)$$

In this control strategy, difference of measured i_{dr} and i_{qr} from their reference values is calculated and are processed by PI controllers and according to equations (15) and (18), for obtaining the rotor voltages reference (v^*_{qr}, v^*_{dr}), values of $\omega_{slip}\left(L_m i_{ms} + \sigma L_r i_{dr}\right)$ and $-\omega_{slip} \sigma L_r i_{qr}$ should be added to v'_{qr} and v'_{dr} respectively.

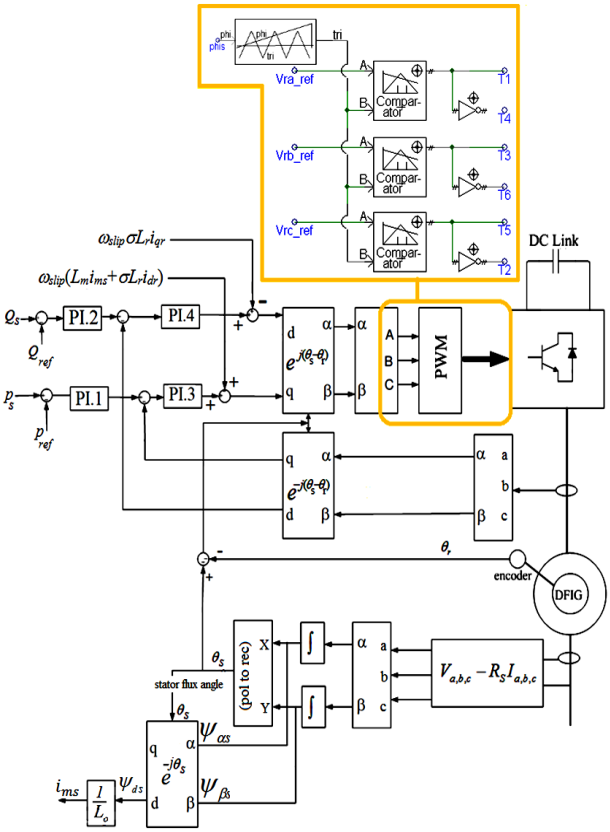

Figure 8. Schematic of the CB-PWM voltage control implementation for rotor side converter

Figure 8 shows control system of rotor side converter with control strategy based on voltage control using carrier based pulse width modulation.

This method is by utilizing Carrier-based Pulse Width Modulation as presented in [7-9]. This is the classical PWM where a reference signal, rotor voltage (V_{ref}), which varies sinusoidally, is compared with a fixed-frequency triangular

carrier waveform (V_{tr}), to create a switching pattern as shown in Figure 9.

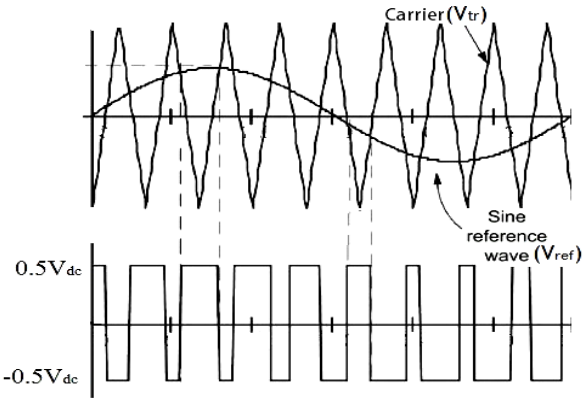

Figure 9. The reference voltage, carrier waveform and the output PWM waveform of a single-phase, two-level VSC

Control of Active and Reactive Power by Hysteresis Current Control

This control system is based on the fact that, in the stator flux oriented frame, the rotor current variations will affect in stator current variations and as mentioned in previous section, by controlling the rotor current, the stator active and reactive powers (P_s, Q_s) can be controlled as indicated in (16). The rotor currents (i_{ra},i_{rb},i_{rc}) of the machine can be resolved into the well known direct and perpendicular components i_d and i_q. Hence the component i_q is used to control the stator active power. The component i_d then controls the reactive power entering the machine. If i_q and i_d can be controlled precisely, then so can the stator side active and reactive powers.[16]

The procedure for ensuring that the correct values of i_d and i_q flow in the rotor is achieved by generating the corresponding phase currents references $i_{ra,ref}$, $i_{rb,ref}$ and $i_{rc,ref}$, and then using a suitable voltage sourced converter (VSC) based current source to force these currents into the rotor.[17],[18]

As shown in Figure 10 a reference current ($i_{rq,ref}$) is derived from the error between the $P_{s,ref}$ and the actual P_s, by tuning a PI controller, Similarly, a reference current ($i_{rd,ref}$) is obtained from the error between the $Q_{s,ref}$ and the present Q_s. Then, both reference currents are transformed to their natural reference frame. These rotor current references, after the d,q to a,b,c transformation, are used for implementing the hysteresis modulation on the rotor side power converter. [19]

Accordingly when the rotor phase current oversteps the upper band, the lower switch of relevant phase is turned on and the upper switch is turned off and vice versa. Thus the difference between the desired and actual currents is kept within the tolerance band as shown in Figure 11. By making the thresholds smaller, the desired current can be approximated to any degree necessary. Note however, that there is a limit to which this can be done, because the smaller the threshold, the smaller the switching periods, i.e., the higher the switching frequency and losses. In this mechanism, the actual current is forced in to track the reference current in its tolerance band continuously. [18-20]

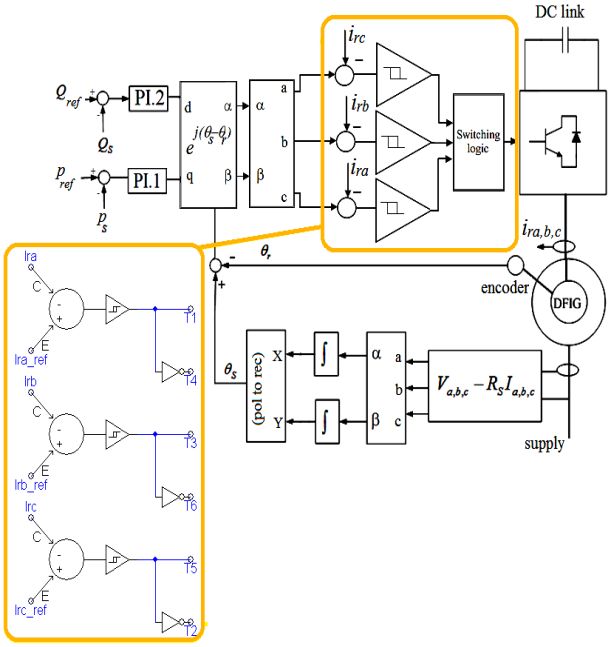

Figure 10.Schematic of the hysteresis current control implementation for rotor side converter

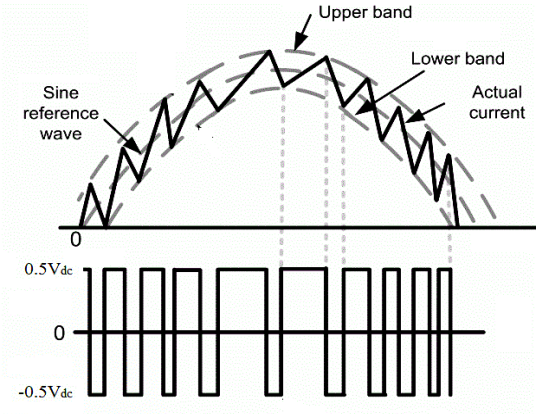

Figure 11. Hysteresis bands around the reference current and the output waveform of a single-phase, two-level VSC

SIMULATION RESULTS

In this section explained control strategies in previous parts, has been simulated on a doubly-fed induction generator and its behavior in different condition has been analyzed. Simulation has been done by PSCAD/EMTDC and the DFIG is rated at 2^{MW} and its parameters have been presented in Table 1.

Main consideration of this thesis is the control strategy of rotor side converter. The network side converter control has been implemented by using of presented strategy in [11] for DC link voltage control. Simulation of rotor side converter control system, which has been explained completely, implemented by DPC, PWM voltage control and hysteresis current control methods, and their dynamical behavior in the steady state has been compared with each other, and benefits and drawbacks of methods have been evaluated.

Table 1.Parameters of the DFIG Simulated

Rated Power	2MW
Stator voltage	690V
Stator/rotor turns ratio	0.3
R_s	0.0108 pu
R_r	0.0121pu (referred to the stator)
L_m	3.362 pu
$L_{\square s}$	0.102 pu
$L_{\square r}$	0.11 pu (referred to the stator)
Lumped inertia constant	0.5
Number of pole pairs	2

The value of reference voltage for DC link is adjusted on 1200^{v} and the capacity of capacitor is $1600^{\mu F}$. Value of the reactance connected serially to the network side converter is 0.25^{mH}. For network side converter, CB-PWM switching strategy is used that frequency of triangular carrier signal is set on 2^{KHz}.

According to Figure 12, during the simulation, DC link voltage is controlled on 1200 volt.

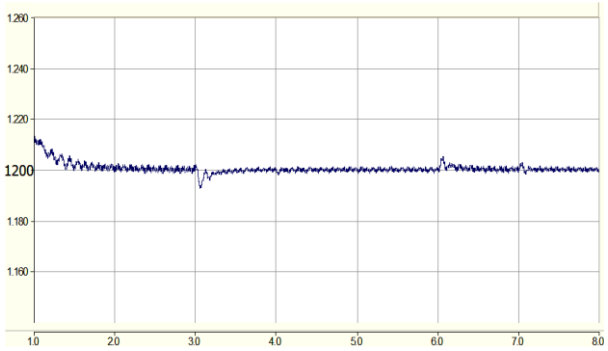

Figure 12. DC link voltage

At first DFIG has been supposed at speed control mode which the speed of rotor is adjusted from outside. In this step, behavior of the generator during variation of rotor speed, from sub-synchronous to super-synchronous, has been shown and the effectiveness and ability of mentioned methods in controlling active and reactive power of wind generator has been assessed.

Considering that flux estimation is only depended on stator resistance, in second step, control strategies performance has been surveyed by changing the stator resistance at range of 0.7 and 1.3 of its rated resistance value.

In the next scenario, the DFIG is assumed in torque control mode, which the input mechanical power of DFIG is provided by a wind turbine, and stator active and reactive power, exchanged rotor active power with network and rotor speed are analyzed. The value of used parameters in control strategies are shown in Table 2. Moreover the band

Table 2. Used Parameters in Control Strategy of PWM Voltage Control and Hysteresis Current Control

Controller parameters of reactive power		Controller parameters of reactive power	
K_{P1}	1.5	K_{P2}	4
T_{I1}	0.48[s]	T_{I2}	0.25[s]
K_{P3}	1.5	K_{P4}	4
T_{I3}	0.48[s]	T_{I4}	0.25[s]

width of hysteresis controller which has been used in current control method, supposed to be 2% of output current of rotor side inverter.

In first stage generator speed has been controlled from outside and simulation results include: stator active and reactive power control, stator current, rotor current, transferred active power of rotor. These results are expressed for three control methods during variations of rotor speed from sub-synchronous to super-synchronous. As it is shown in Figure 13e, during the period of 8.5–11.5 s. the rotor speed increases from 0.85 to 1.15 p.u. Various power steps are also applied, i.e., active and reactive power references are changed from -1.8 to -0.8^{MW} at 9^{s} and from -0.6 to $+0.3^{MVar}$ at 11^{s}. Minus sign for active power means the injection of power to the network and for reactive power means absorbing the power.

Regarding to Figure 13, it can be deduced that the strategy of direct power control the same as the other methods, shows very good performance in this case, as by choosing the hysteresis band width, the ripple of active and reactive power around the reference value can be controlled, While parameters of PI controller, presented in other methods, needs precise and complicated adjustment. In this research, band width of three level hysteresis controllers has been adjusted in 2% of generator rated power so that the ripple of active and reactive power remains in the same range.

Also, in considering Figure 13a, at the moment that power reference changes, DPC method has better dynamical response (about 5ms) comparing with PWM voltage vector (about 25ms).

As shown in Figure 13 the strategy of hysteresis current control executes the same as PWM voltage control. This control method shows an acceptable performance during variations of rotor speed. By choosing the hysteresis band width, the ripple of rotor current and consequently active and reactive power around the reference value can be controlled, While in PWM voltage control method the extra PI controllers requires more precise and complicated adjustment. As mentioned before, in this research, band width of two level hysteresis controllers has been adjusted in 2% of rotor current so that the ripple of rotor current remains in the same range.

As shown in Figure 13d, in speed of sub-synchronous, slip is positive and rotor absorbs active power to network and conversely. During all the time of simulation, frequency of injecting current to rotor is constant and is equal with $s.(f_S)$. When the rotor speed reaches on synchronous, the slip is equal to zero and consequently the rotor active power is zero and so frequency of injected current to rotor is zero (Figure 13c,d).

In next section the value of stator resistance, applied in the simulation for estimating the stator flux, have been allocated 70% and 130% of the rated value to determine the robustness of methods despite the error in the stator resistance value estimation. References of active power at second 3, has a step change from -0.8 to 1.8^{MW} and reference of reactive power at second 5, has one step change from -0.6 to 0.6^{MVar}. As we can see in Figure 14, active and reactive power tracking is performed in all of methods. The control strategy of PWM voltage control in addition to stator resistance needs precise information of other parameters of the machine such as rotor and stator inductance and also mutual inductance; while in applying the direct power control method and hysteresis current control, the stator resistance, is needed as an input

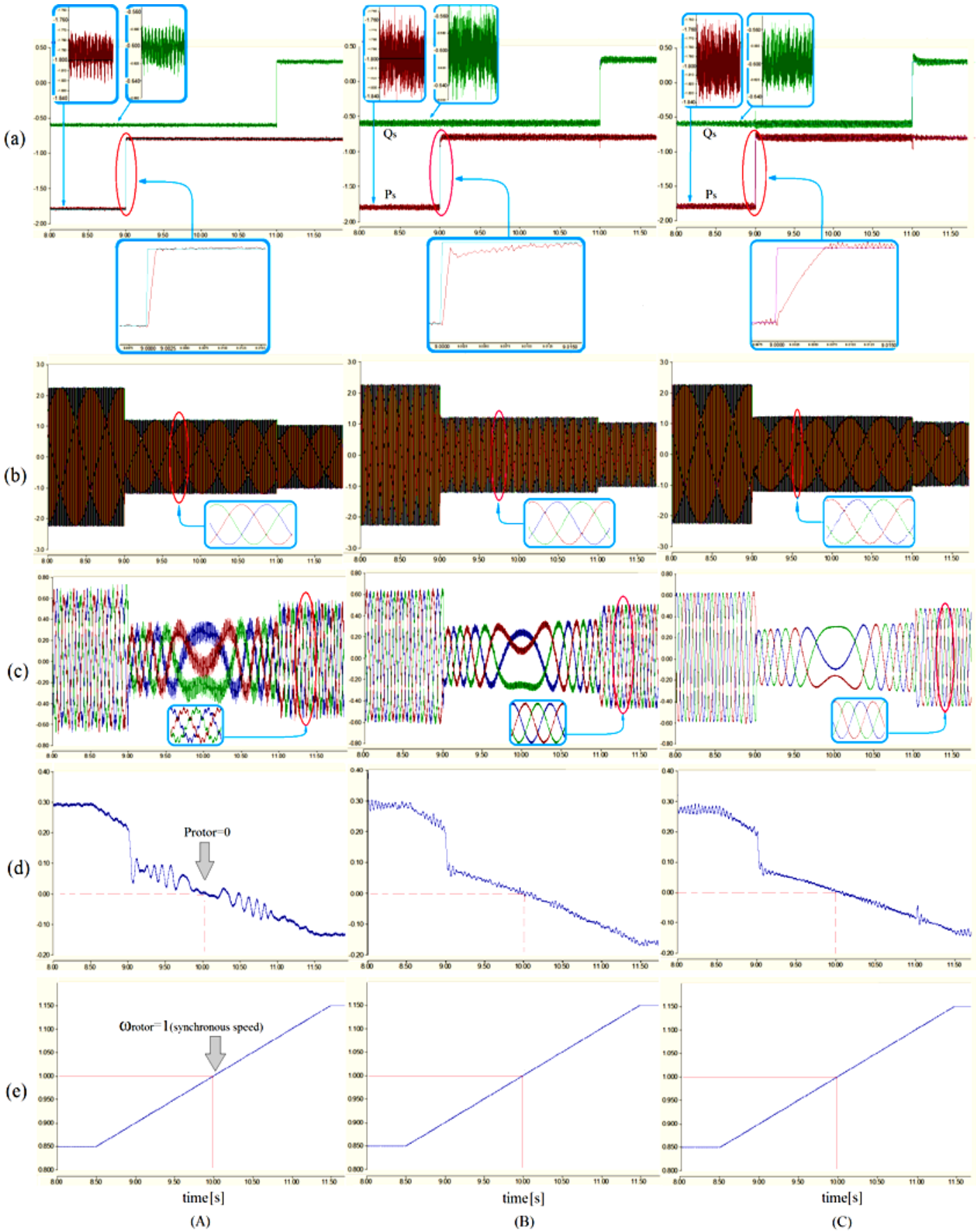

Figure 13. Simulated results under various stator active and reactive power steps and rotor speed variation with (A) DPC (B) voltage control using CB-PWM and (C) hysteresis current control strategy: (a)stator active power input (MW) and reactive power output (MVar), (b)three phase stator current (kA), (c)three phase rotor current (kA), (d) rotor active power input (MW), (e) rotor speed (p.u) (In all of figure groups the left column figures are "A", the middle column figures are "B" the right figures are "C")

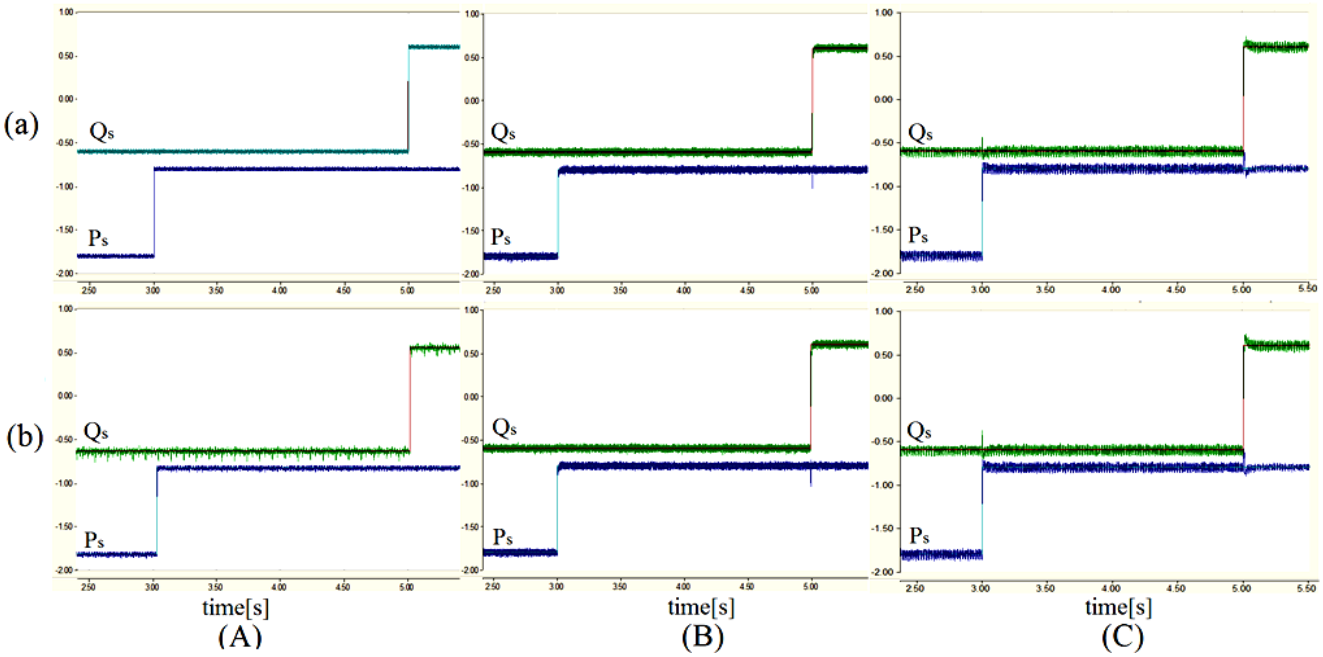

Figure 14.Simulated results under various stator active and reactive power steps with (A) DPC and (B) voltage control using CB-PWM and (C) hysteresis current control strategy: (a) stator active power input (MW) and reactive power output (MVar) With 30 percent more resistance and; (b)with 30 percent less resistance than rated stator resistance

parameter, which usually is estimated. Results show that the error caused by estimation of this parameter, do not decrease the effectiveness of these methods.

In next stage, the DFIG is studied in mode of torque control. In this step a wind turbine has been simulated to provide the mechanical input power of DFIG and its parameters are presented in Table 3.

Table 3. Wind Turbine Parameters

rated power of wind turbine (MVA)	2^{MVA}
Length of wind turbine blades	40^{M}
air density	$1.229^{Kg/m3}$
Gear ratio	80

At 3^{s}, the wind velocity changes from 11.57 $^{m/s}$ (in this velocity the turbine generates its rated power) to $9^{m/s}$ and at second 6 changes to 10.5 $^{m/s}$. In the first case the stator active power reference is 0.9 of mechanical power, and in the next case it is 1.1 of output mechanical power of turbine. In this case the following results are: the stator active and reactive power exchange, the rotor active power and the speed of rotor.

References of active power at 4^{s}, has one step change from zero to 0.5^{MW} and at 7^{s} changes to -0.5^{MW}.

Simulation results in torque control mode, for mentioned strategies are shown in Figure 15 where the active power reference equal to the 0.9 of mechanical input power.

As shown in Figure 15a when the machine is in torque control mode, the tracking of both active and reactive power is well done in either of strategies. Moreover, according to (18), since the stator active power reference equal to 0.9 of mechanical power input, the rotor injects active power into the network to balance the power. This is clearly seen in Figure 15b. In this mode, the rotor speed is super-synchronous and Figure 15c illustrates this point.

$$P_m = P_s + P_r \tag{18}$$

Once more the simulation is accomplished for the case that the stator active power reference equal to 1.1 of mechanical power of the turbine. Since the stator active power reference equal to 1.1 of mechanical power input, the rotor absorbs active power from the network to balance the power. The rotor speed in this case is sub-synchronous. These issues can be seen in Figure 16.

CONCLUSION

In this research control of active and reactive power of a doubly-fed induction generator have been surveyed by using three control methods based on using direct power control, voltage control carrier based pulse width modulation (CB-PWM) and hysteresis current control, and then the results have been compared with each other in different scenarios.

First simulation section shows the performance of mentioned strategy during variations of rotor speed from sub-synchronous to super-synchronous. In simulation results we can see that all these mentioned methods have very good performance during variation of rotor speed, as in DPC the ripple of active and reactive power around the reference value can be controlled directly by choosing the hysteresis band width, While parameters of PI controller, presented in CB-PWM voltage control and hysteresis current control, needs precise and complicated adjustment. However, the hysteresis current control is recommended than voltage control because; it offers the advantages of reduced proportionate integral (PI) controllers at the rotor side converter, and less intricacies of controller design. In other words, hysteresis control operation requires to perceive only the output currents, and needs no adjustments. Also in hysteresis current control strategy by choosing the hysteresis band width, the ripple of rotor

current and consequently active and reactive power around the reference value can be controlled. Therefore rotor current waveform can be synthesized which brings control of instantaneous current waveform, peak current protection and high accuracy.

In applying the direct power control method, the stator resistance, is needed as an input parameter, which usually is estimated. In the second section the value of stator resistance, applied in simulation, have been allocated 70% and 130% of the rated value to determine the robustness of methods despite the error in stator resistance value estimation. Results show that the error caused by estimation of this parameter, do not decrease the effectiveness of this method. In the next step, doubly-fed induction generator in torque control mode is surveyed and obtained results show that direct power control, not only is simple, but also has faster dynamic response and good performance in different conditions.

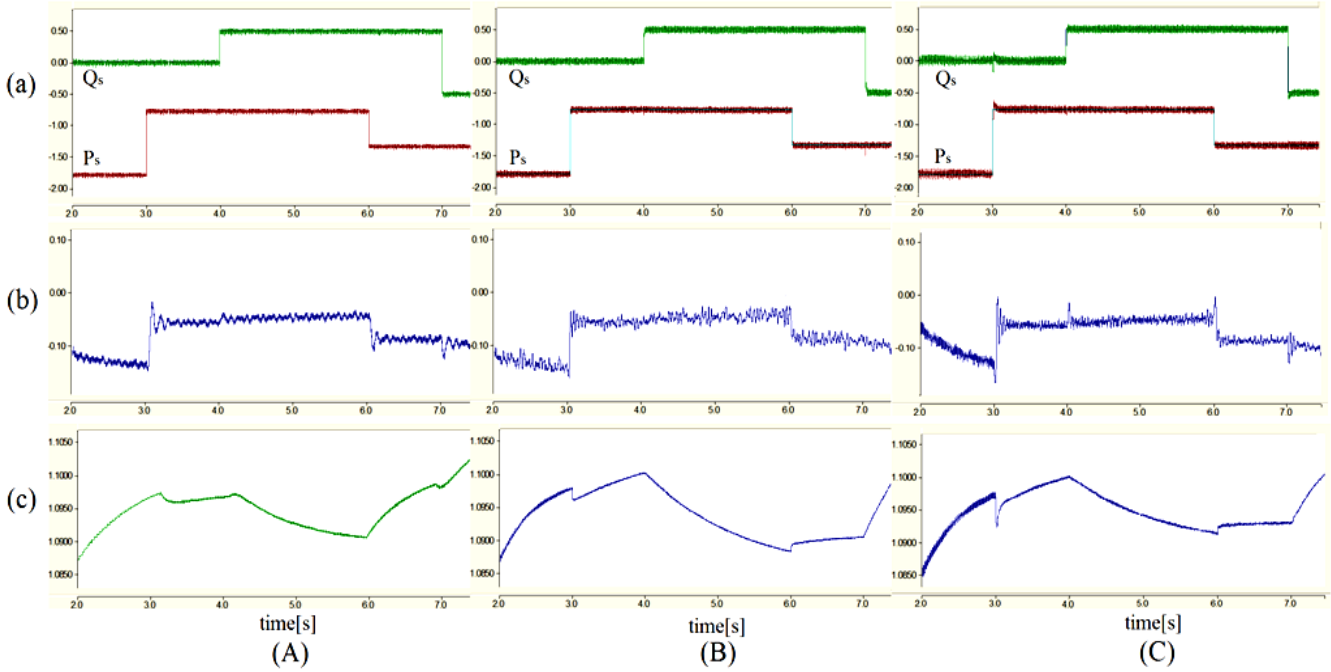

Figure 15. Simulated results with step change in mechanical input torque and under stator reactive power and active power reference adjusted to of 0.9 P_m(mechanical input power) with (A) DPC and (B) voltage control using CB-PWM and (C) hysteresis current control strategy: (a) stator active power input (MW) and reactive power output (MVar), (b) rotor active power input (MW), (c) rotor speed (p.u)

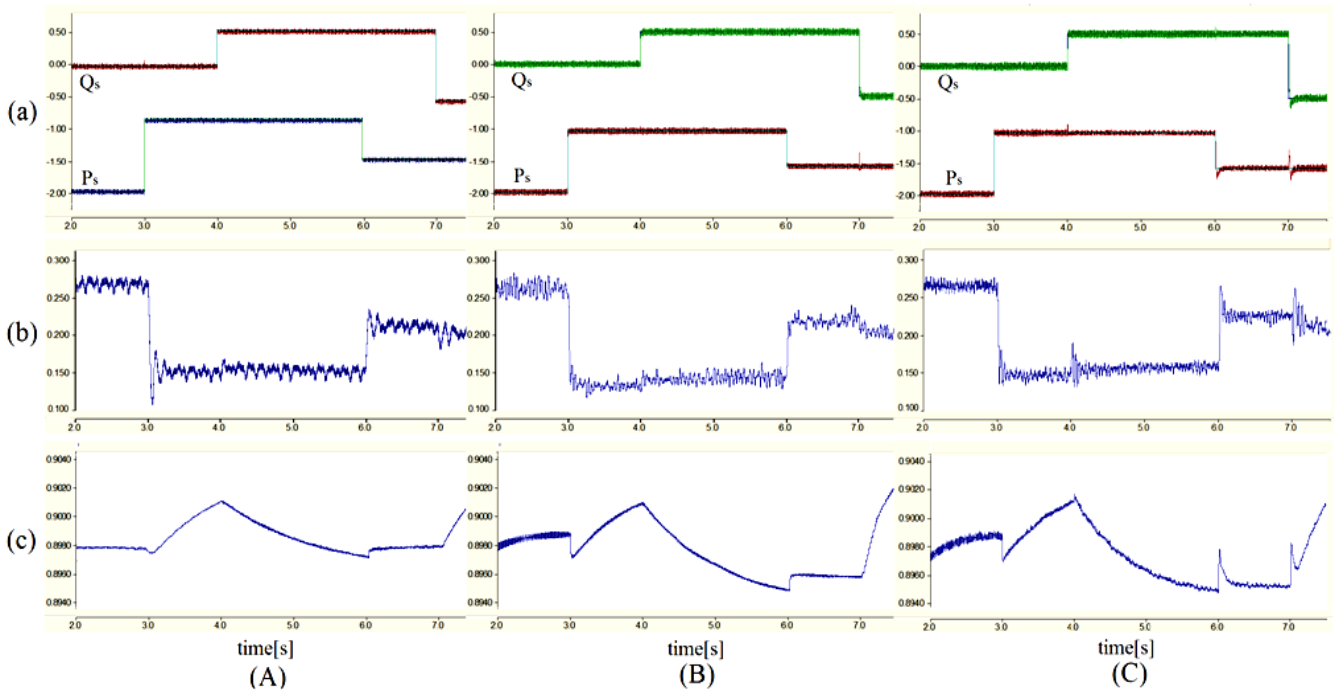

Figure 16. Simulated results with step change in mechanical input torque and under stator reactive power and active power reference adjusted to of 1.1 P_m(mechanical input power) with (A) DPC and (B) voltage control using CB-PWM and (C) hysteresis current control strategy: (a) stator active power input (MW) and reactive power output (MVar), (b) rotor active power input (MW), (c) rotor speed (p.u)

REFERENCES

[1] L. H. Hansen, L. Helle, F. Blaabjerg, E. Ritchie, S. Munk-Nielsen, H. Bindner, P. Sørensen, and B. Bak-Jensen, "Conceptual survey of generators and power electronics for wind turbines," Risø National Laboratory, Roskilde, Denmark, Tech.Rep. Risø-R-1205(EN), ISBN 87-550-2743-8, Dec. 2001

[2] L. Morel, H. Godfroid, A. Mirzaian, and J. Kauffmann, "Double-fed induction machine: converter optimization and field oriented control without position sensor," IEE Proc.Electr. Power Appl., vol. 145, no. 4, pp. 360–368, July 1998

[3] L. Xu and C. Wei, "Torque and reactive power control of a doubly fed induction machine by position sensorless scheme," IEEE Trans. Ind. Applicat. , vol. 31, no. 3, pp. 636–642, May/June 1995.

[4] J.F. Manwell, J.G. McGowan, and A. L. Rogers, "Wind Energy Explained: Theory, Design and Application", John Wiley & Sons, ISBN 978-0-470-01500-1, (first published 2009)

[5] O. Anaya-Lara, N. Jenkins, J. Ekanayake, P. Cartwright and M. Hughes "Wind Energy Generation: Modeling and Control", John Wiley & Sons, ISBN 978-0-470-71433-1, New York, NY, USA, 2009

[6] G. Abad, J. López, M. A. Rodríguez, L. Marroyo, G. Iwanski, "Doubly Fed Induction Machine: Modeling and Control for Wind Energy Generation", John Wiley & Sons, ISBN: 9781118104965, Sep. 2011

[7] L. Xu and P. Cartwright, "Direct active and reactive power control of DFIG for wind energy generation", IEEE Trans. Energy Conversion, Vol. 21, No. 3, pp. 750-758, September. 2006

[8] D. Santos-Martin, J. Rodriguez-Amenedo, and S. Arnalte, "Direct power control applied to doubly fed induction generator under unbalanced grid voltage conditions", IEEE Trans. Power Electronics Vol.23, No.5, pp. 2328-2336, 2008

[9] P. Zhou, Y. He and D. Sun, "Improved direct power control of a DFIG based wind turbine network unbalance," IEEE Trans. on Power Systems, Vol. 24, No.11, pp. 2465-2474, November. 2009

[10] A.J. Sguarezi Filho, M.E. de Oliveira Filho and E. Rubbert Filho, "A predictive power control for wind energy", IEEE Trans. Sustainable Energy, Vol. 2, No. 1, pp. 97-105, January. 2011

[11] R. Pena, J. Clare and G. Asher, "Doubly fed induction generator using back-to-back PWM converters and its application to variable speed wind-energy generation", "IEE Proc. Electric Power Application, Vol. 143, No. 3, pp. 231-241, May. 1996

[12]A. Tapia, G. Tapia, J. Ostolaza, , and J. Saenz, \Modeling and control of a wind turbine driven doubly fed induction generator," IEEE Transactions on Energy Conversion, vol. 18, no. 2, pp. 194-204, Jun. 2003

[13]D. Chwa and K. Lee "Variable Structure Control of the Active and Reactive Powers for a DFIG in Wind Turbines" IEEE Trans, Vol. 46, No. 6, pp. 2545-2555 Nov /Dec, 2010

[14]A. Tapia, G. Tapia, J. X. Ostolaza, and J. R. Saenz, "Modeling and control of a wind turbine driven doubly fed induction generator," IEEE Trans. Energy Convers. , vol. 18, no. 2, pp. 194–204, Jun. 2003.

[15]Y. Lei, A. Mullane, G. Lightbody, and R. Yacamini, "Modeling of the wind turbine with a doubly fed induction generator for grid integration studies," IEEE Trans. Energy Convers. , vol. 21, no. 1, pp. 257–264, Mar. 2006.

[16] B. Chowdhury and S. Chellapilla, "Doubly-fed induction generator control for variable speed wind power generation," Electric Power Systems Research, vol. 76, no. 9, pp. 786-800, Jun. 2006

[17]M.P. Kazmierkowski, L.Malesani, "Current control techniques for three-phase voltage source PWM converters: a survey", Industrial Electronics, IEEE Transactions on industrial Electronics,Vol.45, No.5, Oct.1998.,pp.691-703

[18] P. N. Tekwani, R. S. Kanchan, and K. Gopakumar, "Current-error space vector-based hysteresis PWM controller for three-level voltage source inverter fed drives," Proc. Inst.Electr. Eng. Electric Power Applications, vol. 152, no. 5, pp. 1283–1295, Sep. 200

[19] Y. Tang and L. Xu, "A Flexible Active and Reactive Power Control Strategy for a Variable Speed Constant Frequency Generating System", IEEE Transactions on Power Electronics, Vol.10, No. 4, pp.472-478, July/Aug., 1995,

[20] L. Chang, R. Doraiswami, T. Boutot, and H. Kojabadi, "Development of a wind turbine simulator for wind energy conversion systems," in Canadian Conference on Electrical and Computer Engineering, vol. 1, pp. 550-554, Mar. 2000